A thermodynamic model for tunable multi-shape memory effect and cooperative relaxation in amorphous polymers

Haibao Lu[a,*], Xiaodong Wang[a], Kai Yu[b], YongQing Fu[c] and Jinsong Leng[a]

[a]Science and Technology on Advanced Composites in Special Environments Laboratory, Harbin Institute of Technology, Harbin 150080, China

[b]Department of Mechanical Engineering, University of Colorado Denver, Denver, CO 80217, United States

[c]Faculty of Engineering and Environment, University of Northumbria, Newcastle upon Tyne, NE1 8ST, UK

*Corresponding author, E-mail: luhb@hit.edu.cn

Abstract: By integrating phase transition theory and Takayanagi principle, we have developed a thermodynamic model to describe working mechanism and thermomechanical behavior of shape memory polymers (SMPs) with tunable multi-shape memory effect (multi-SME). Thermodynamics and state/phase transitions of different segments in the SMPs were modeled by considering their cooperative relaxation, which is defined as a process where a group of segments undergo relaxation simultaneously, based on the Takayanagi principle. Dependences of thermomechanical behavior of amorphous polymers on volume fraction, cooperative relaxation and glass transition temperatures of both hard and soft segments were theoretically investigated. Working mechanisms of the multi-SME and cooperative relaxation of the amorphous polymers have well been explained using this newly proposed model, which offers an effective approach for designing new SMPs with

multi-segments.

Keywords: shape memory polymer, dynamic response, multi-shape memory effect

1. Introduction

Shape memory polymers (SMPs) are one of the classical smart materials which possess excellent properties including large elastic strain, light weight, low cost and biocompatibility [1-6]. SMPs have been widely used in aerospace engineering, medicine, sensors and actuators [7-12]. Most types of the SMPs are amorphous [13-15], and these amorphous SMPs are generally made up of hard segments and soft segments [16,17]. The hard segment plays a critical role to memorize the permanent shapes and orientations of macromolecules, whereas the soft segment has the ability to response to the external stimulus and generate a transition from a "frozen" state to an active one [18,19]. The macromolecule chains which are composed of both the hard and soft segments could retain the permanent shape from their temporary one, therefore possessing a good shape memory effect (SME) [18,19]. Furthermore, multi-shape memory effect (multi-SME) can be generated in the macromolecule chains by combining one type of hard segment and several types of soft segments, the latter of which could help to fix and keep the various temporary shapes [20-24]. As presented in the previous papers, triple-SME has been realized in the SMPs which are incorporated of one hard segment and three soft segments [25-29].

Multi-SME in polymers is expected to significantly extend their practical and potential applications [25-27]. However, it is difficult to theoretically model and predict their thermomechanical and shape recovery behaviors of multi-SME in polymers owing to the complexity of their macromolecule structures, their thermal transitions and relaxation among the segments [28,29]. Meanwhile, the theoretical models are critical to investigate the multi-SMEs for new types of amorphous SMPs and explore their constitutive relationships between multi-glass transitions and shape recovery behaviors.

Previously, we have established a static model to describe the unique molecular and structural characteristics of the SMPs after the transition process [23,24]. However, as far as we know, the dynamic transition and cooperative relaxation of the multi-SME have so far never been theoretically discussed. The cooperativity is defined as the degree of a group of segments to undergo relaxations simultaneously in a macromolecule [30-33], and the segmental relaxation can be determined from the intermolecular cooperativity [34]. In this article, we have, for the first time, studied working mechanisms and thermomechanical behaviors of the multi-SME by integrating phase transition theory with the Takayanagi model [35,36]. Both series-parallel model and parallel-series model were developed to characterize the dynamically thermal transition and cooperative relaxation of the SMPs with multi-segments. Dependences of thermomechanical behaviors on volume fraction, cooperative relaxation and glass transition temperatures of the segments have been

theoretically investigated. Finally, effects of cooperative relaxation on the thermomechanical behavior of the SMP have been discussed.

2. Model of the SME in SMP

According to the phase transition theory, soft segment is composed of both the frozen phase and active phase. The frozen phase transforms into the active phase when temperature is increased into the phase transition zone. However, the influence of the hard segment on SMP's modulus has not been considered in the above theory before. Therefore, the current phase transition model [18] does not present the stress-strain relationship among the different components due to the lack of incorporation of dynamic transition and cooperative relaxation of the different segments. However, it is critical to establish a dynamic model to describe the synergistic and cooperative effects of the hard segment and soft ones on the thermomechanical properties of the SMPs.

In the first step, the SMP incorporated of a hard segment and a soft one is considered and discussed. The volume fraction of frozen phase in soft segment (W_s) as a function of temperature can be written as [18],

$$W_s = 1 - \frac{1}{1 + C_f (T_h - T)^n} \tag{1}$$

where C_f and n are the phenomenological material constants [18]. When the temperature reaches to a high temperature (T_h), the frozen soft segment has been completely transformed into the active one. Following the Takayanagi principle [23,35], ϕ ($0 \le \phi \le 1$) is introduced as the dimensionless cross-sectional area perpendicular to the direction of deformation, and λ ($0 \le \lambda \le 1$) is introduced as the

dimensionless length along the direction of deformation. In both the series-parallel model and parallel-series model, functions of ϕ and λ can be used to present the volume fractions of the hard and soft segments in the SMP macromolecules, as illustrated in Figures 1(a) and 1(b), respectively. Meanwhile, the soft segment and its dynamic transition are presented by the frozen soft segment (symbol F) and the active one (symbol A).

[Figure 1]

2.1 Series-parallel model

As presented in Figure 1, we have the following relationship,

$$\lambda_1 + \lambda_2 + \lambda_3 = 1 \tag{2}$$

where λ_1 is a constant and indicates the dimensionless length along the direction of deformation of the hard segment. Meanwhile, λ_2 and λ_3 are those for the active soft segment and frozen one, respectively.

In the series-parallel model, the dimensional cross-sectional area perpendicular to the direction of deformation (ϕ) is unchanged. Therefore, we can obtain,

$$W_s = \frac{\lambda_3}{\lambda_2 + \lambda_3} \tag{3}$$

Integrating equations (2) and (3) into equation (1), we can use the constant λ_1 to express the variable functions λ_2 and λ_3 as a function of temperature:

$$\lambda_2 = \frac{1-\lambda_1}{1+C_f(T_h - T)^n}, \quad \lambda_3 = 1 - \frac{1-\lambda_1}{1+C_f(T_h - T)^n} - \lambda_1 \tag{4}$$

where $C_f = 2.76\times10^{-5}(1/K^4)$, n=4 and $T_h = 358K$ [18]. We can set the dimensionless length along the direction of deformation of the hard segment (λ_1)

equals to 0, 0.2, 0.4, 0.6 and 0.8, respectively. As revealed in Figures 2(a) and 2(b), the values of λ_2 and λ_3 change correspondingly with the increase of λ_1. The value of λ_2 increases slowly with temperature at the initial phase transition process but then increases sharply at the temperature range from 330 to 350K until reaching a plateau value, at different given constants of λ_1=0, 0.2, 0.4, 0.6 and 0.8, respectively. On the other hand, value of λ_3 decreases with an increase in temperature, which is more significant at temperatures above 300K.

[Figure 2]

Based on the Takayanagi principle [37] and the series-parallel model, the mechanical properties of two phases as a function of temperature can be written as:

$$\frac{1}{E(T)}=\frac{\phi}{\lambda E_s(T)+(1-\lambda)E_h}+\frac{1-\phi}{E_h} \tag{5}$$

where $E_s(T)$ is the modulus of soft segment. E_h is the modulus of hard one, and it is a constant at the transition temperature range.

From equation (5), we can obtain the boundary conditions of the SMP's modulus in the phase transition process. At the initial stage, we can define $E_s(T)$=E_f (E_f is the modulus of the frozen phase and is considered as a constant). When the temperature reaches T_h, we now have E_s=E_a (E_a is the modulus of the active phase and is also considered as a constant). Therefore, equation (5) could be regarded as the boundary conditions for the beginning and final transitions of the gloss modulus of SMP.

For the dynamic transition of the soft segment, E_h of the hard segment is kept as a constant [23]. Therefore, equation (5) could be rewritten as,

$$\frac{1}{E(T)} = \frac{\phi}{\lambda_1 E_h + \lambda_2 E_a + \lambda_3 E_f} + \frac{1-\phi}{E_h} \tag{6}$$

Combining equations (4) and (6), the modulus of SMP with the increase of temperature can be re-written as:

$$\frac{1}{E(T)} = \frac{\phi}{\lambda_1 E_h + \frac{1-\lambda_1}{1+C_f(T_h-T)^n} E_a + (1 - \frac{1-\lambda_1}{1+C_f(T_h-T)^n} - \lambda_1) E_f} + \frac{1-\phi}{E_h} \tag{7}$$

The volume fraction of the hard segment (W_h) could be written as,

$$W_h = 1 - \phi + \phi\lambda_1 \tag{8}$$

To investigate the effects of hard segment on the dynamic modulus, it is assumed that $E_h = E_f = 5E_a$ and $W_h = 0.6$. The dimensionless cross-sectional area (e.g., ϕ) is increased from 0.4, 0.6, 0.8 to 1.0, respectively, as shown in Figure 3(a). The simulation results of moduli obtained using the series-parallel model are between those obtained from the single parallel connection and those from single series connection. With an increase in value of ϕ, the dynamic modulus of SMP tends to be more close to that obtained from the series connection. In the phase transition process, the modulus of single series connection is lower than that obtained from the single parallel connection at the same temperature.

We then further study the influence of dimensionless length λ_1 of the hard segment (which is in series connection with the soft segment) on the modulus of SMP. The calculated results obtained from the equation (7) are shown in Figure 3(b). With the increase of dimensionless length, it is found that the dynamic modulus of SMP increases at the same temperature because the increase of hard segment (which is in series connection with soft segments) will cause the increase of the modulus. Based

on the series-parallel model, parameters of ϕ and λ obtained from the series connection have more significant effects on the dynamic modulus of SMP than those obtained from the parallel connection.

[Figure 3]

Effects of volume fraction of hard segment (W_h) on the storage modulus of the SMP will be studied further. We set $\phi = 0.6$ and $W_h = 0.4$ (0.5, 0.6, 0.7 or 0.8), respectively, as shown in Figure 4(a), while $\lambda = 0.4$ and $W_h = 0.4$ (0.6, 0.8 or 1.0), respectively, as shown in Figure 4(b). With an increase of the volume fraction of hard segment which is in series connection with the soft region, the dynamic modulus is sharply increased. The dynamic modulus is much larger at the same temperature when more volume fraction of hard segment is in series connection with the soft segment.

To further investigate the influence of the volume fraction of hard segment (which is in parallel connection with the soft segment) on the modulus, we fixed the series parameter λ to be 0.4. Analysis results showed that with an increase of the volume fraction of the hard segment, the dynamic modulus increases at the same temperature. Results showed that the hard segment in the series connection has a more significant influence on the dynamic modulus as a function of temperature than that in the parallel connection. Both these two different types of connections make SMP more stiffness thus helping to fix the shape of SMP easily.

[Figure 4]

The simulation results of the storage modulus as a function of temperature can be compared with the experimental data determined by the dynamic mechanical analysis

(DMA) [38], and the comparison results are shown in Figure 5 . Figures 5(a) and 5(b) plot the numerical results obtained from the series-parallel model and parallel-series model, respectively, while the experimental data are also plotted for comparisons. All the material parameters used in the proposed model could be determined from the DMA results, and they can then be used to describe and predict the experimental results of the storage modulus as a function of temperature. Results show that the results obtained from the theoretical model fit well with the experimental results.

[Figure 5]

2.2 Parallel-series model

From Figure 2, we can obtain,

$$\phi_1 + \phi_2 + \phi_3 = 1 \tag{9}$$

where ϕ_1 is a constant which is the dimensionless area perpendicular to the direction of deformation of the hard segment; while ϕ_2 and ϕ_3 are those of the active phase and the frozen phase in the soft segment, respectively.

For the parallel-series model, the dimensionless cross-sectional area of the hard segment is assumed unchanged. Therefore, we can obtain,

$$W_s = \frac{\phi_3}{\phi_2 + \phi_3} \tag{10}$$

The equations (9) and (10) can be integrated with equation (2), and a constant (ϕ_1) can be used to express the variable function (ϕ_2 and ϕ_3), thus we now have:

$$\phi_2 = \frac{1-\phi_1}{1+C_f(T_h - T)^n}, \quad \phi_3 = 1 - \frac{1-\phi_1}{1+C_f(T_h - T)^n} - \phi_1 \tag{11}$$

Based on the Takayanagi principle [38], the parallel-series model of two phases

could be written as,

$$E=(1-\lambda)(\frac{\phi}{E_h}+\frac{1-\phi}{E_s})^{-1}+\lambda E_h \tag{12}$$

Similarly, equation (12) can be assumed to describe the moduli of the SMP for the start and complete transition stages using the parallel-series model.

During the dynamic transition of the soft segment, the hard segment is assumed to be unchanged. So equation (12) could be rewritten as,

$$E(T)=(1-\lambda)(\frac{\phi_1}{E_h}+\frac{\phi_2}{E_a}+\frac{\phi_3}{E_f})^{-1}+\lambda E_h \tag{13}$$

Integrating equation (11) into equation (13), the dynamic modulus of SMP with the increase of temperature has the following form,

$$E(T)=(1-\lambda)(\frac{\phi_1}{E_h}+\frac{\frac{1-\phi_1}{1+C_f(T_h-T)^n}}{E_a}+\frac{1-\frac{1-\phi_1}{1+C_f(T_h-T)^n}-\phi_1}{E_f})^{-1}+\lambda E_h \tag{14}$$

Based on the parallel-series model, the volume fraction of the hard segment can be written as,

$$W_h=\lambda+\phi_1-\lambda\phi_1 \tag{15}$$

where parameter λ indicates the effect of series connection caused by the hard segment. The parameter λ and the volume fraction of the hard segment (W_h) are kept unchanged for both the series-parallel model and the parallel-series one. Figure 6 compares the differences of the results obtained from the two models. During the analysis, we set λ=0.05, 0.2, 0.4, 0.5 and W_h=0.6, respectively. Results showed that the dynamic modulus obtained from the parallel-series model decreases more quickly at the initial process of increasing temperature if compared with that obtained from

the series-parallel model under the same series volume fraction of hard segment. Therefore, compared with the series-parallel model, the parallel-series connections formed between the soft segment and the hard segment accelerate the SME of the SMP at the beginning of phase transition. It is beneficial for the fast responses of the SMP upon changing the temperature.

Moreover, the modulus values obtained from the parallel-series model are much less than those obtained from the series-parallel model at the same transition temperature range, which indicates that it's more favorable to trigger phase transition of the SMP under the parallel-series condition.

[Figure 6]

During free recovery process, the change of the temperature-dependent recovery strain of SMP has the similar form as equations (7) and (14) for series-parallel and parallel-series model, respectively [31]. We can get the following form for recovery strain in series-parallel model and parallel-series one, respectively,

$$\frac{1}{\varepsilon(T)}=\frac{\phi}{\lambda_1\varepsilon_h+\frac{1-\lambda_1}{1+C_f(T_h-T)^n}\varepsilon_a+(1-\frac{1-\lambda_1}{1+C_f(T_h-T)^n}-\lambda_1)\varepsilon_f}+\frac{1-\phi}{\varepsilon_h} \tag{16}$$

$$\varepsilon(T)=(1-\lambda)(\frac{\phi_1}{\varepsilon_h}+\frac{\frac{1-\phi_1}{1+C_f(T_h-T)^n}}{\varepsilon_a}+\frac{1-\frac{1-\phi_1}{1+C_f(T_h-T)^n}-\phi_1}{\varepsilon_f})^{-1}+\lambda\varepsilon_h \tag{17}$$

where $\varepsilon(T)$ is the recovery strain of polymer, ε_h, ε_a and ε_f are the recovery strain of hard region, active phase and frozen phase, respectively. Comparisons between the theoretical results and experimental data [38] have been presented in Figures 7(a) and 7(b). The material parameters used in the equations (16) and (17) are

the same with those in the equations (13) and (14). It is found that the simulation results of obtained from the series-parallel model are in a good agreement with the experimental ones. The recovery strain is mainly determined by the phase transition of the polymer. Results show that the active phase and frozen phase of multiple soft segments prefer to connect with each other in the series connections.

[Figure 7]

From the discussion in Figure 7, the series-parallel model is more accurate to describe the free recovery strain of SMP with the increase of temperature. We further investigate the stress evolutions with respect to temperature at the constrained recovery process based on the series-parallel model. At temperature *T*, the uniaxial stress ($\sigma(T)$) is,

$$\sigma(T) = \varepsilon(T) \cdot E(T) \tag{18}$$

The recovery strain of the hard phase is small compared with one in the soft phase, to simplify the constitutive modelling, we simplify equation (16) by neglecting the effect of the hard phase on the recovery strain, and is rewritten as follows,

$$\varepsilon(T) = \frac{1}{1 + C_f (T_h - T)^n} \varepsilon_{pre} \tag{19}$$

where ε_{pre} is the pre-deformed strain at high temperature. Equation (19) also has a form,

$$\varepsilon(T) = \left(1 - \frac{1}{1 + C_f (T_h - T)^n}\right) \varepsilon_s \tag{20}$$

where ε_s is the stored strain at low temperature.

Equation (7) is determined by the DMA experiments, however, the thermal

recovery process is temperature-dependent, and then the change of modulus is decayed. So we introduce temperature T_r to replace $C_f(T_h - T)^n$ with $C_f(T_h - T + T_r)^n$ and take equation (7) and equation (19) into equation (18), we can get the stress evolutions with respect to temperature,

$$\sigma(T) = \left[\frac{\phi}{\lambda_1 E_h + \frac{1-\lambda_1}{1+C_f(T_h - T + T_r)^n} E_a + (1 - \frac{1-\lambda_1}{1+C_f(T_h - T + T_r)^n} - \lambda_1) E_f} + \frac{1-\phi}{E_h} \right]^{-1} \cdot \frac{1}{1+C_f(T_h - T)^n} \varepsilon_{pre} \quad (21)$$

To verify the correction of series-parallel model, we compare this model with experimental data [39] of the storage modulus, free recovery strain and the stress evolutions at the constrained condition with respect to temperature by the same values of the involved parameters in Figure 8(a), 8(b) and 8(c), respectively. The simulation parameters are shown in Table 1. The high temperature (T_h) during the DMA experiment is 317.79*K* in Figure 8(a) which is lower than $T_h = 333K$ in free recovery experiment in Figure 8(b), mainly caused by the thermal rate and the shape memory behavior is time-dependent, so we introduce parameter T_r in equation (21) to show the decay change of the storage modulus at the constrained recovery condition. In Figure 8(a), WLF equation is used to transfer the frequency (*f*) into temperature to compare the experimental data with equation (7), and the WLF parameters $C_1 = 6.9$, $C_2 = 87.9^\circ C$ and $T_{ref} = 80^\circ C$ [39]. Equation (20) is used to describe the free recovery of the stored strain ($\varepsilon_s = 0.2$) with temperature in Figure 8(b). The viscoelastic change of the strain is caused by the release of the stored strain with the processing of the phase transition in soft phase. At last, the experimental data of the

stress evolutions with respect to temperature is compared with equation (21) in Figure 8(c). The simulation curves of the storage modulus, free recovery strain and constrained stress evolutions with respect to temperature fit well with experimental data at the same values of involved parameters.

[Table 1]

[Figure 8]

3. Thermodynamic model of tunable multi-SME

Figures 9(a) and 9(b) show illustrations of the multi-SME of SMP whose soft segments and hard segment are in series-parallel connection and parallel-series connection with the hard segment, respectively.

[Figure 9]

Based on Figure 9, the cooperative relaxation and corresponding changes of modulus of the multi-SMP with temperature are further studied. According to the series-parallel model, equation (7) could be rewritten as,

$$\frac{1}{E(T)}=\frac{\phi}{\lambda E_h+\sum_{i=1}^{n}[\frac{\lambda_i}{1+C_{fi}(T_{hi}-T)^{n_i}}E_{ai}+(\lambda_i-\frac{\lambda_i}{1+C_{fi}(T_{hi}-T)^{n_i}})E_{fi}]}+\frac{1-\phi}{E_h} \quad (22)$$

where i represents different soft segments and n represents the number of the soft segments.

Based on the parallel-series model, equation (14) could be further rewritten as,

$$E(T)=(1-\lambda)\left(\frac{\phi}{E_h}+\sum_{i=1}^{n}(\frac{\frac{\phi_i}{1+C_{fi}(T_{hi}-T)^{n_i}}}{E_{ai}}+\frac{\phi_i-\frac{\phi_i}{1+C_{fi}(T_{hi}-T)^{n_i}}}{E_{fi}})\right)^{-1}+\lambda E_h \quad (23)$$

To study the influences of the fixed hard segment and varied soft segments on the

dynamic modulus in SMP, the numerical analysis was performed with two different soft segments, and the results are shown in Figure 10. We keep the volume fraction of the hard segment (W_h) fixed at 0.5, whereas we set: $E_h = E_{f1} = E_{f2} = 5E_{a1} = 5E_{a2}$, $T_{h1} = 350K$ and $T_{h2} = 400K$. Figure 10(a) shows the dynamic modulus data obtained from the series-parallel model with $\lambda = 0$, 0.1, 0.2, 0.3, 0.4, 0.5 and $\lambda_1 = \lambda_2$. With the increase of the volume fractions of the hard segments which are in series connection with the soft segments, the dynamic modulus is increased at the given temperature. It also shows two-stage phase transition processes with the increase of temperature. When the value of λ equals to 0.5, the SMP (with hard and soft segments connected in the series-parallel connection model) presents a shape recovery behavior as the same as that obtained from the series connection model. At the same volume fraction of the hard segment, the modulus of SMP obtained from the series-parallel connection model reveals a rapid decrease in comparison with that from the series connection.

Figure 10(b) shows the results from the parallel-series connection of one hard segment and two soft segments. Unlike the series-parallel model, the decrease of the modulus of the second phase transition process is not obvious in the parallel-series model. It indicates that the parallel-series connection is ineffective to trigger the multi-phase transition in the SMP. Meanwhile, the reduction of the modulus by forming a parallel connection is more significant than the series connection based on the parallel-series model. This clearly indicates that the series connection of the hard segment with soft regions prevents the occurrence of multi-SME. This phenomenon

happens more apparently in the second phase transition process.

[Figure 10]

To investigate the influence of volume fraction of hard segment (W_h) on the dynamic modulus, we set W_h = 0.3, 0.45, 0.6, 0.75 and 0.9, respectively and the calculation results are shown in Figure 11. The dimensionless cross-sectional area of the series connection (ϕ) equals to 0.8 for the case shown in Figure 11(a). By increasing the volume fraction of the hard segment which is in series connections with the two soft segments, the dynamic modulus does not show obvious changes with the increase of temperature. Meanwhile, the modulus of SMP increases with the increase of the volume fraction of the hard segment at the same temperature. Figure 11(b) indicates increasing the volume fraction of the hard segment which is parallel with the soft segment has the same effect on the dynamic modulus, if compared with the series connection. However, increasing the volume fraction of the hard segment which is in the parallel connection with the soft segment does not show apparent influence on the second phase transition compared with the results obtained from those shown in Figure 11(a). Results clearly indicate that increasing the volume fraction of the hard segment which is in parallel connection with the soft segment is an effective way to increase the modulus of multi-SMP based on the series-parallel model. Also this will not apparently affect the multi-SMEs in the SMP.

Using the parallel-series model, results presented in Figures 11(c) and 11(d) show the similar result. Increasing the volume fraction of the hard segments which are in series connection with the soft segments will not cause apparent multi-SME, although

this will affect more on the second phase transition process. Therefore, increasing the volume fraction of the hard segment which is in parallel connection with the soft segment is the best way to increase the modulus of multi-SME obtained from both the models. Finally, results also show that the series-parallel model will result in a more significant multi-SME compared with the parallel-series model with different volume fractions of the hard segment.

[Figure 11]

To verify of the simulation results using the proposed model, the experimental data [40] obtained from a triple-SME are used for comparison, as shown in Figure 12. As presented in the previous work [40], a two stage shape recovery of epoxy-based SMP occurred at 330 K and 350 K. The moduli of the hard segment, and the two active segments are E_h =1554.31MPa, E_{a1} =60MPa and E_{a2} =20MPa, respectively. The other materials parameters determined from the DMA measurements are listed in Table 2. Here, the simulation results of the parallel-series model are employed to predict the elastic modulus as a function of temperature. Results show that the volume fraction of the soft phase in the first stage transition is much less than that in the second stage transition. The initial recovery process of the second stage transition is not apparent because the change of the modulus is small insignificant compared with that of the first stage transition. Results show that the simulation results of series-parallel model are in a good agreement with the experimental ones.

[Table 2]

[Figure 12]

Figure 13 investigates the cooperation relaxation process of the SMP. We set the complete transition temperatures into four different soft segments: e.g., $T_{h1}=330K$, $T_{h2}=340K$, $T_{h3}=360K$, $T_{h4}=400K$, based on two models. Results show that if the transition temperature ranges of two soft segments are very close between each other, the multi-SME becomes unobvious with the increase of temperature. This suggests that the occurrence of multi-SME is strongly dependent upon the temperature interval of each soft segment. Using the parallel-series model, the calculated modulus decreases significantly at the initial stage but the decrease rate becomes much lower afterwards, indicating that the multi-SME is not obvious for the parallel-series connection mode. Clearly, the numerical analysis suggests that the series-parallel model is more suitable to describe the mechanisms of the multiple shape memory behavior and describe the cooperation relaxation process of different soft segments.

[Figure 13]

From the above discussions, the series-parallel model is more suitable to describe the occurrence of the multi-SME. Based on the series-parallel model, effect of the transition temperature interval of two soft segments on the multi-SME was further studied and the results are shown in Figure 14. The reference temperature is set to be T_{h1}=310K, T_{h2}=340K, $T_{h3}=370K$, $T_{h4}=400K$ and $T_{h5}=430K$. It is clear that the dynamic modulus is changed linearly in the identical temperature interval for the different soft segments. With the increase of temperature interval between two near transition stages, the SME becomes more obvious. This series-parallel model is useful

for the design of the multi-SME in SMPs a variety of transition temperature interval of the different soft segments.

[Figure 14]

In summary, the parallel-series model is more suitable for describing the single SME whose connection mode accelerates the decrease of modulus compared with that from the series-parallel model. Whereas the occurrence of the multi-SME needs a low volume fraction of hard segment which is in series with the different soft segments. A better way to increase the modulus of multi-SMPs is to increase the volume fraction of the hard segments which are in parallel connection with soft segments. Different soft segments which are in series connection with each other will have a better effect on multi-SME than those from the parallel connection. Meanwhile, the relaxation temperature interval for different soft segments should be extended to a proper range to enable the SMPs with multi-SME.

4. Conclusions

In this study, a dynamic model was proposed to describe the unique characteristics of the mechanisms of multi-SME for the dynamic phase transition of different soft segments with the increase of temperature. Both the series-parallel model and the parallel-series model were used to investigate the working mechanisms of multi-SME in amorphous SMPs. Effects of the volume fraction and connection mode of hard segment on the multi-SME were systematically studied. Based on the phase transition theory, effects of molecular structure characteristics on the dynamic changes of modulus were further investigated. From the numerical analysis of our

proposed series-parallel and parallel-series model, we obtain the design principle in molecular scale which is favorable to trigger the multi-SME in the amorphous SMPs. This study is expected to provide a powerful tool to understand the working mechanism and provide theoretical guidance for the design of multi-SME in SMPs.

Acknowledgements

This work was financially supported by the National Natural Science Foundation of China (NSFC) under Grant No. 11672342 and 11725208, Newton Mobility Grant (IE161019) through Royal Society and the NSFC, and Royal academy of Engineering UK-Research Exchange with China and India.

References

[1] Lendlein A, Jiang H Y, Jünger O and Langer R 2005 Light-induced shape-memory polymers *Nature* **434** 879–882

[2] Mather P T, Luo X F and Ingrid A 2007 Rousseau Shape Memory Polymer Research *Annual Review of Materials Research* **39** 445-471

[3] Xie T 2011 Recent advances in shape memory polymer *Polymer* **52** 4985-5000

[4] Hu J L, Zhu Y, Huang H H and Lu J 2012 Recent advances in shape–memory polymers: Structure, mechanism, functionality, modeling and applications *Progress in Polymer Science* **37** 1720-1763

[5] Meng H and Lia G Q 2013 A review of stimuli-responsive shape memory polymer composites *Polymer* **54** 2199-2221

[6] Sun L, Huang W M, Ding Z, Zhao Y, Wang C C, Purnawali H and Tang C 2012 Stimulus-responsive shape memory materials: A review *Materials & Design* **33** 577-640.

[7] Lan X, Liu Y J, Lv H B, Wang X H, Leng J S and Du S Y 2009 Fiber reinforced shape-memory polymer composite and its application in a deployable hinge

Smart Materials and Structures **18** 024002.

[8] Lendlein A and Langer R 2002 Biodegradable, Elastic Shape-Memory Polymers for Potential Biomedical Applications *Science* **296** 1673-1676

[9] Wache H M, Tartakowska D J, HentrichM A and Wagner H 2003 Development of a polymer stent with shape memory effect as a drug delivery system *Journal of Materials Science: Materials in Medicine* **14** 109-112

[10] Horn J, Hwang W, Jessen S L, Keller B K, Miller M W, Tuzun E, Hartman J, Clubb F J and Maitland D J 2017 Comparison of shape memory polymer foam versus bare metal coil treatments in an in vivo porcine sidewall aneurysm model *Journal of Biomedical Materials Research Part B: Applied Biomaterials* **105** 1892-1905

[11] Li G Q and Shojaei A 2012 A viscoplastic theory of shape memory polymer fibres with application to self-healing materials *Proceedings of the Royal Society A: Mathematical, Physical & Engineering Sciences* **468** 2319-2346

[12] Maitland D J, Metzger M F, Schumann D, Lee A and Wilson T S 2002 Photothermal properties of shape memory polymer micro-actuators for treating stroke *Lasers in Surgery and Medicine* **30** 1-11

[13] Nguyen T D, Qi H J, Castro F and Long K N 2008 A thermoviscoelastic model for amorphous shape memory polymers: Incorporating structural and stress relaxation *Journal of the Mechanics and Physics of Solids* **56** 2792-2814

[14] Mao Y Q, Yu K, Isakov M S, Wu J T, Dunn M L and Qi H J 2015 Sequential self-folding structures by 3D printed digital shape memory polymers *Scientific Reports* **5** 13616

[15] Yu K, Ge Q and Qi H J 2014 Reduced time as a unified parameter determining fixity and free recovery of shape memory polymers *Nature Communications* **5** 3066

[16] Tobushi H, Hara H, Yamada E and Hayashi S 1996 Thermomechanical properties in a thin film of shape memory polymer of polyurethane series *Smart Materials and Structures* **5** 483-491

[17] Alteheld A, Feng Y K, Kelch S and Lendlein A 2005 Biodegradable, amorphous

copolyester-urethane networks having shape-memory properties *Angewandte Chemie International Edition* **44** 1188-1192

[18] Liu Y P, Gall K, Dunn M L, Greenberg A R and Diani J 2006 Thermomechanics of shape memory polymers: Uniaxial experiments and constitutive modeling *International Journal of Plasticity* **22** 279-313

[19] Lu H B, Wang X D, Yao Y T and Fu Y Q 2018 A "frozen volume" transition model and working mechanism for the shape memory effect in amorphous polymers *Smart Materials and Structures* **27** 065023

[20] Xie T 2011 Tunable polymer multi-shape memory effect *Nature* **464** 267-270

[21] Sun L and Huang W M 2010 Mechanisms of the multi-shape memory effect and temperature memory effect in shape memory polymers *Soft Matter* **6** 4403-4406

[22] Yu K, Xie T, Leng J S, Ding YF and Qi H J 2012 Mechanisms of multi-shape memory effects and associated energy release in shape memory polymers *Soft Matter* **8** 5687-5695

[23] Lu H B, Yu K, Huang W M and Leng J S 2016 On the Takayanagi principle for the shape memory effect and thermomechanical behaviors in polymers with multi-phases *Smart Materials and Structures* **25** 125001.

[24] Lu H B, Wang X D, Yu K, Huang W M, Yao Y T and Leng J S 2017 A phenomenological formulation for shape/temperature memory effect in amorphous polymers with multi stress components *Smart Materials and Structures* **26** 095011

[25] José M. Cuevas, Raquel Rubio, Lorena Germán, José M. Laza, José L. Vilas, Matilde Rodriguez and Luis M. León. Triple-shape memory effect of covalently crosslinked polyalkenamer based semicrystalline polymer blends. Soft Matter, 2012, 8, 4928-4935.

[26] Junjun Li and Tao Xie. Significant impact of thermo-mechanical conditions on polymer triple-shape memory effect. Macromolecules, 2011, 44 (1), pp 175-180.

[27] Samuel C, Barrau S, Lefebvre J M, Raquez J M and Dubois P 2014 Designing multiple-shape memory polymers with miscible polymer blends: evidence and origins of a triple-shape memory effect for miscible PLLA/PMMA blends

Macromolecules **47** 6791-6803

[28] Ware T, Hearon K, Lonnecker A, Wooley K L, Maitland D J and Voit W 2012 Triple-shape memory polymers based on self-complementary hydrogen bonding *Macromolecules* **45** 1062-1069

[29] Zhao J, Chen M, Wang X Y, Zhao X D, Wang Z W, Dang Z M, Ma L, Hu G H and Chen F H 2013 Triple shape memory effects of cross-linked polyethylene/polypropylene blends with cocontinuous architecture *ACS Applied Materials and Interfaces* **5** 5550-5556

[30] Matsuoka S 1997 Entropy, free volume, and cooperative relaxation *The Journal of Research of NIST* **102** 213-228

[31] Saito H, Miyashita H and Inoue T 1992 Cooperative chain relaxation in a single-Phase mixture of dissimilar polymers: definition and implication of the cooperativity *Macromolecules* **25** 1824-1827

[32] Ngai K L and Paluch M 2003 Inference of the evolution from caged dynamics to cooperative relaxation in glass-formers from dielectric relaxation data *The Journal of Physical Chemistry B* **107** 6865-6872

[33] Cerveny S, Schwartz G A, Bergman R and Swenson J 2004 Glass transition and relaxation processes in supercooled water *Physics Review Letters* **93** 245702

[34] Matsuka S and Quan X 1991 A model for intermolecular cooperative in conformational relaxations near the glass transition *Macromolecules* 24 2770-2779

[35] Takayanagi M, Imada K and Kajiyama T 1967 Mechanical properties and fine structure of drawn polymers *Journal of Polymer Science C* **15** 263-281

[36] Takayanagi M and Nitta K 1997 Application of a tie molecule model to the postyielding deformation of crystalline polymers *Macromolecular Theory and Simulation* **6** 181-195

[37] Ward I M and Sweeney J 2004 An Introduction to the Mechanical Properties of Solid Polymers (West Sussex: Wiley) 174-183

[38] Shojaei A and Li G 2014 Thermomechanical constitutive modelling of shape memory polymer including continuum functional and mechanical damage effects

Proceedings of the Royal Society A **470** 20140199

[39] Arrieta S, Diani J and Gilormini P 2014 Experimental characterization and thermoviscoelastic modeling of strain and stress recoveries of an amorphous polymer network Mech. Mater **68** 95–103

[40] Xie T, Xiao X and Cheng YT 2009 Revealing triple-shape memory effect by polymer bilayers *Macromolecular Rapid Communications* **30** 1823-1827

Table caption

Table 1. Material parameters for equation (7), (20) and (21)

Table 2. Material parameters for equation (23)

Table 1. Material parameters for equation (7), (20) and (21)

$C_f\ (1/K^n)$	n	ϕ	λ_1	$E_a(MPa)$	$E_f(MPa)$	$E_h(MPa)$	$T_r(K)$
$2.45*10^{-5}$	4.26	0.887	0.018	2.1	636.719	636.71	7.79

Table 2. Material parameters for equation (23)

λ	ϕ	ϕ_1	ϕ_2	C_{f1}	C_{f2}	n_1	n_2
2.83×10^{-6}	0.3	0,173	0.527	7.36×10^{-12}	9.80×10^{-9}	9.87	10.76

Figures caption

Figure 1. (a). Illustrations of the dynamic transition in the soft segment based on the series-parallel model. (b). Illustrations of the dynamic transition in the soft segment based on the parallel-series model

Figure 2. Numerical analysis of (a) λ_2 and (b) λ_3 values with the increase of temperature at different values of λ_1

Figure 3. Theoretical analysis of influences of the dimensionless cross-sectional area (ϕ) and length (λ) of hard segments (which are in series connection with soft segment) on the modulus. (a) $\phi = 0.4, 0.6, 0.8, 1$. (b) $\lambda_1 = 0, 0.05, 0.2, 0.4, 0.6$

Figure 4. Numerical analysis of the effect of volume fraction of hard segment on the dynamic modulus. (a) $\phi = 0.6$, (b) $\lambda = 0.4$

Figure 5. The comparison between experimental data [38] of the change of the storage modulus as a function of temperature with our theoretical model. (a) series-parallel model. (b) parallel-series model

Figure 6. Comparisons between results from the series-parallel model and the parallel-series model, and the orange dashed lines are used to present the numerical result zone of the theoretical models. (a) $\lambda = 0.05$, (b) $\lambda = 0.2$, (c) $\lambda = 0.4$ (d) $\lambda = 0.5$

Figure 7. The comparison between experimental data [38] of the change of the recovery strain with the increase of temperature with our theoretical model. (a) series-parallel model. (b) parallel-series model

Figure 8. Comparison between experimental data of acrylate amorphous network [39] and simulation curve. (a) Storage modulus with the increase of temperature,(b) Free recovery strain with the increase of temperature. (c) Stress evolutions with respect to the temperature at constrained condition

Figure 9. (a). Illustrations of the dynamic transition of SMP with multiple soft segments based on the series-parallel model. (b). Illustrations of the dynamic transition of SMP with multiple soft segments based on the parallel-series model

Figure 10. Numerical analysis results of the connection modes on the dynamic modulus at the same volume fraction of the hard segment; (a) series-parallel model, (b) parallel-series model

Figure 11. Numerical analysis of the influence of volume fraction of the hard segment on the dynamic modulus in (a) and (b) series-parallel model and (c) and (d) parallel-series model

Figure 12. The comparison between experimental data [40] of the modulus and the simulation results of parallel-series model for triple-SMP with two transition behaviors

Figure 13. Numerical analysis results of the cooperative relaxation behavior happened in different temperature intervals based on the series-parallel model and the parallel-series model

Figure 14. Numerical analysis results on the effect of the transition temperature interval between two soft segments on the multi-SME

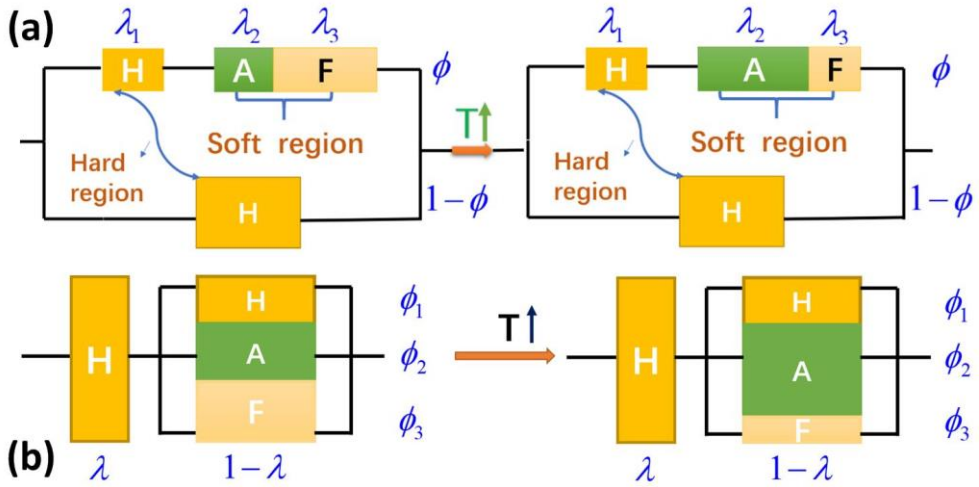

Figure 1. (a). Illustrations of the dynamic transition in the soft segment based on the series-parallel model. (b). Illustrations of the dynamic transition in the soft segment based on the parallel-series model

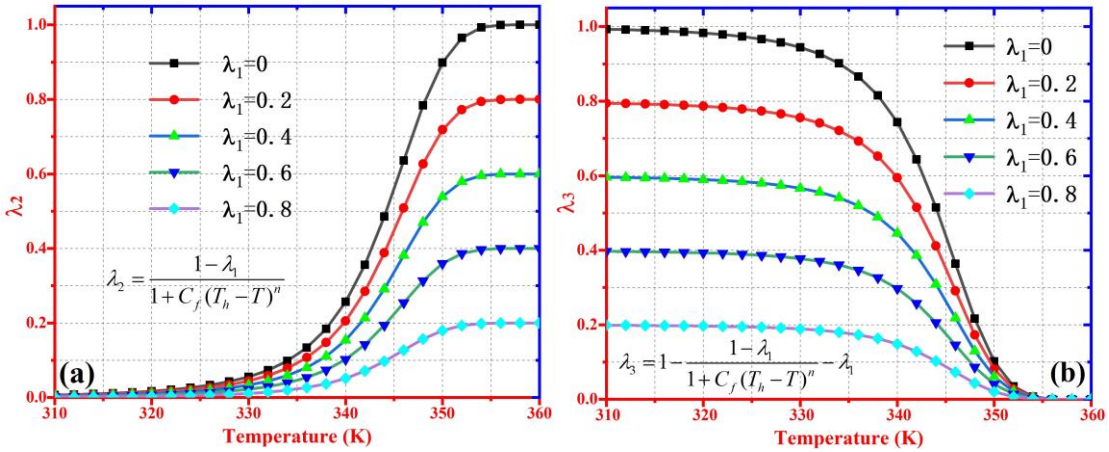

Figure 2. Numerical analysis of (a) λ_2 and (b) λ_3 values with the increase of temperature at different values of λ_1

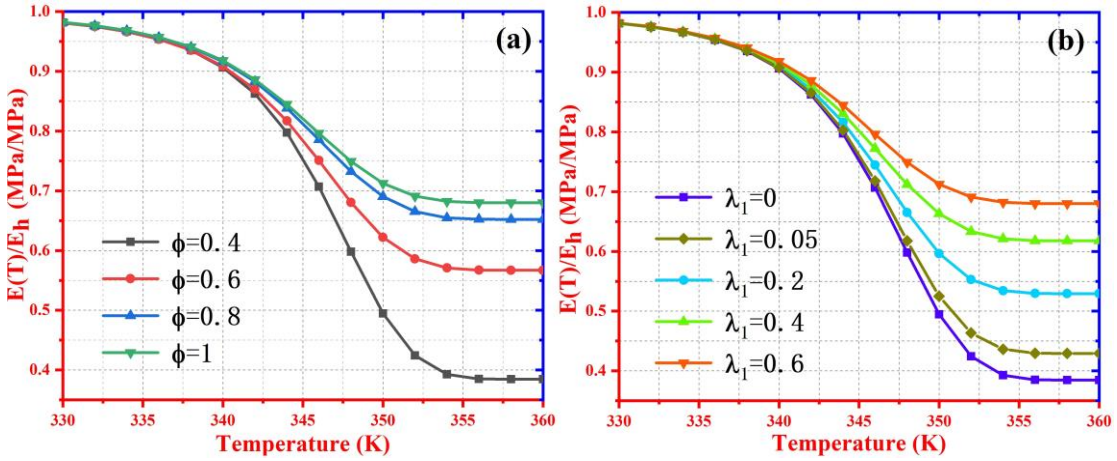

Figure 3. Theoretical analysis of influences of the dimensionless cross-sectional area (ϕ) and length (λ) of hard segments (which are in series connection with soft segment) on the modulus. (a) $\phi = 0.4, 0.6, 0.8, 1$. (b) $\lambda_1 = 0, 0.05, 0.2, 0.4, 0.6$

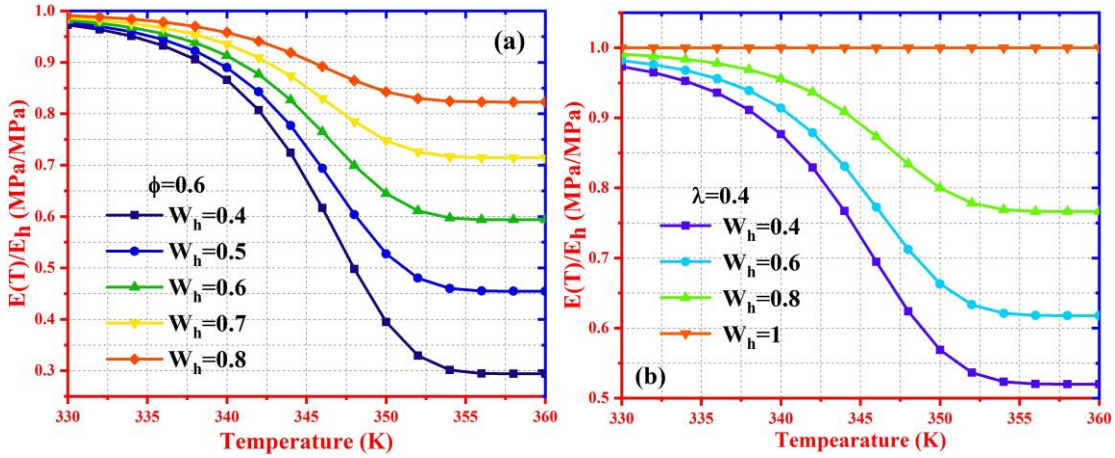

Figure 4. Numerical analysis of the effect of volume fraction of hard segment on the dynamic modulus. (a) $\phi = 0.6$, (b) $\lambda = 0.4$

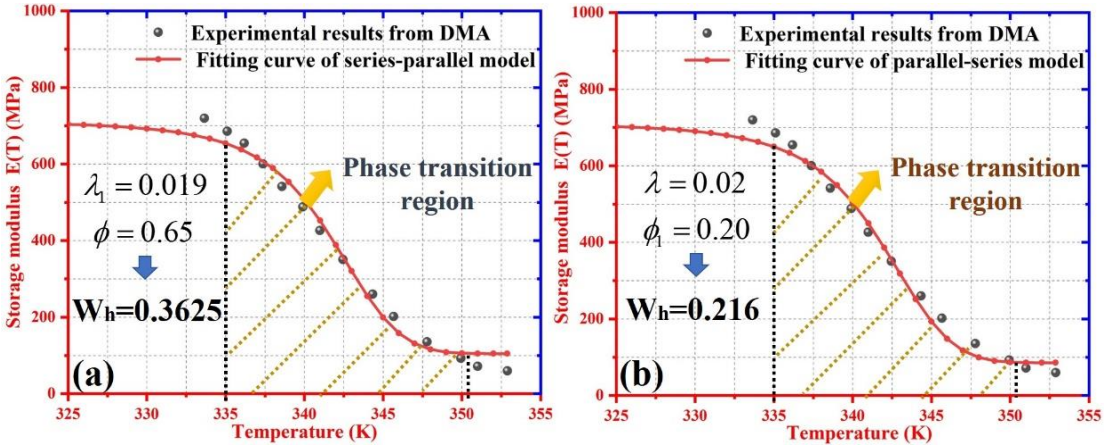

Figure 5. The comparison between experimental data [38] of the change of the storage modulus as a function of temperature with our theoretical model. (a) series-parallel model. (b) parallel-series model

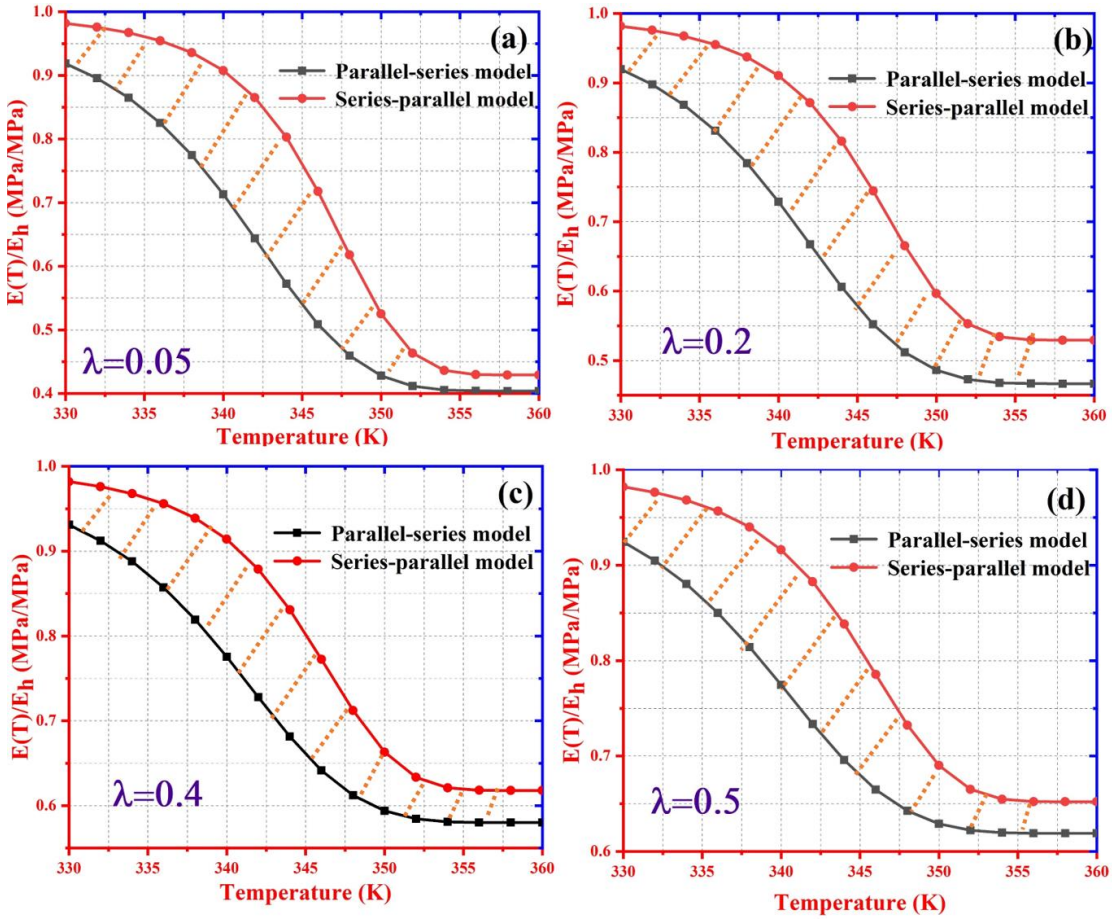

Figure 6. Comparisons between results from the series-parallel model and the parallel-series model, and the orange dashed lines are used to present the numerical result zone of the theoretical models. (a) $\lambda = 0.05$, (b) $\lambda = 0.2$, (c) $\lambda = 0.4$ (d) $\lambda = 0.5$

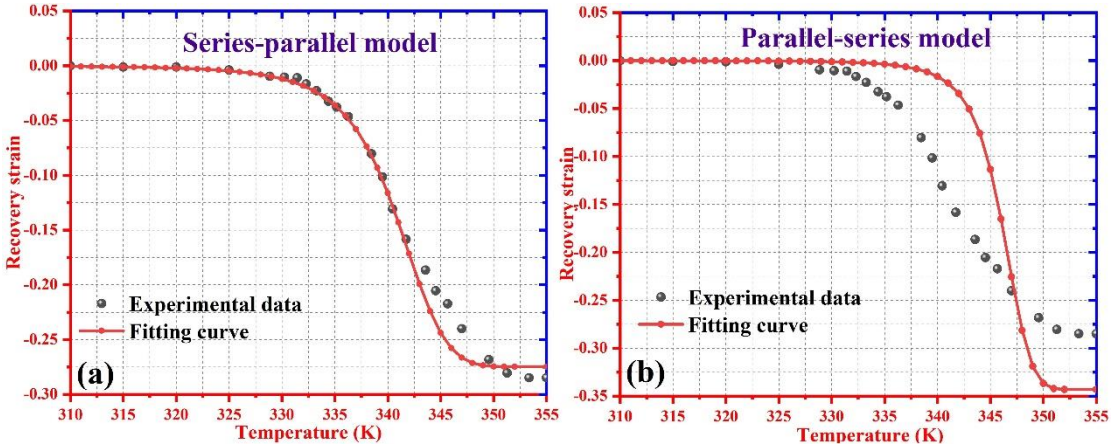

Figure 7. The comparison between experimental data [38] of the change of the recovery strain with the increase of temperature with our theoretical model. (a) series-parallel model. (b) parallel-series model

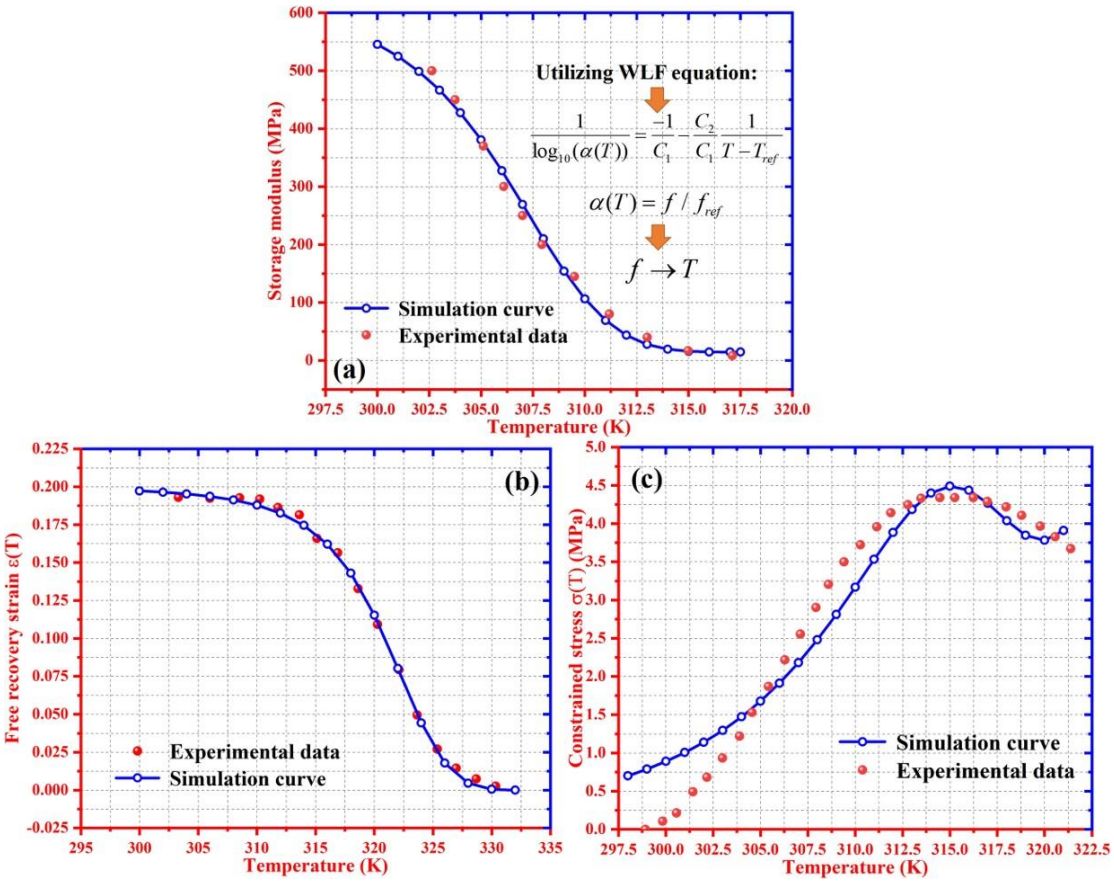

Figure 8. Comparison between experimental data of acrylate amorphous network [39] and simulation curve. (a) Storage modulus with the increase of temperature,(b) Free recovery strain with the increase of temperature. (c) Stress evolutions with respect to the temperature at constrained condition

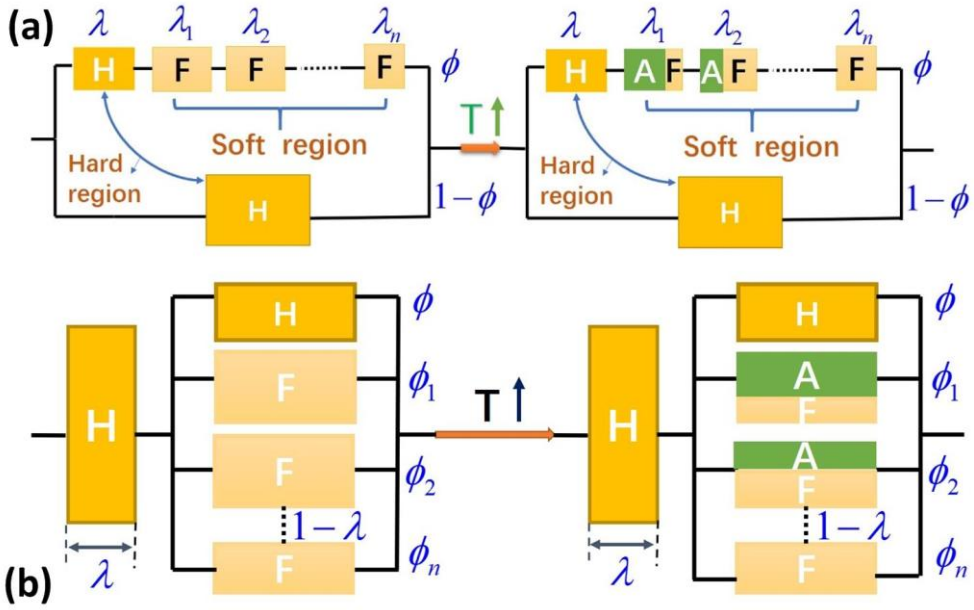

Figure 9. (a). Illustrations of the dynamic transition of SMP with multiple soft segments based on the series-parallel model. (b). Illustrations of the dynamic transition of SMP with multiple soft segments based on the parallel-series model

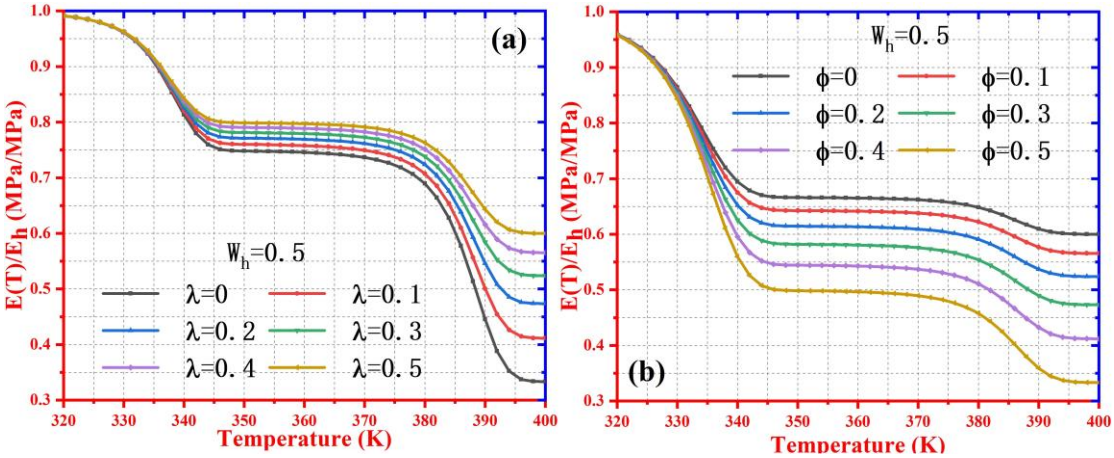

Figure 10. Numerical analysis results of the connection modes on the dynamic modulus at the same volume fraction of the hard segment; (a) series-parallel model, (b) parallel-series model

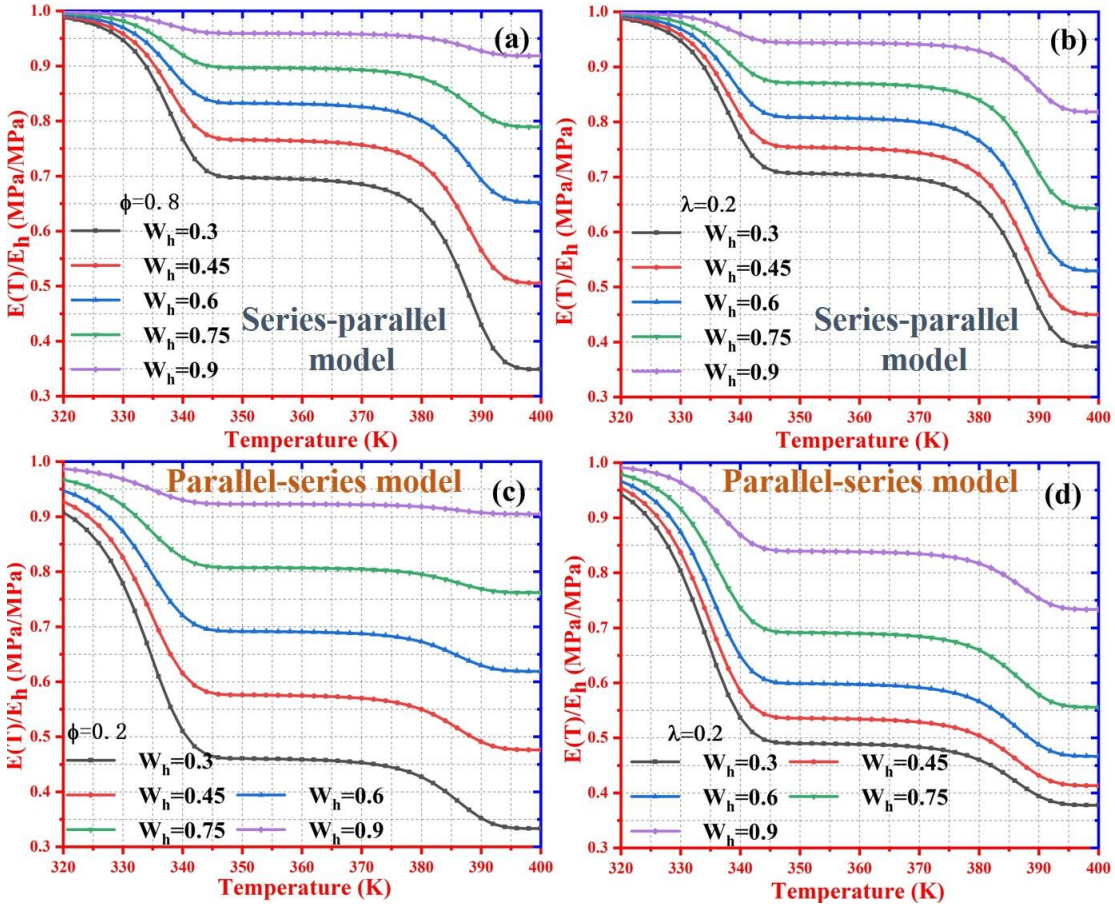

Figure 11. Numerical analysis of the influence of volume fraction of the hard segment on the dynamic modulus in (a) and (b) series-parallel model and (c) and (d) parallel-series model

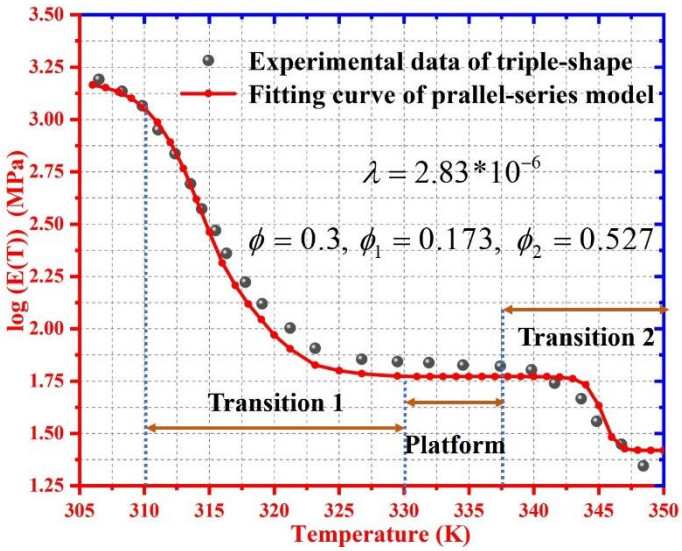

Figure 12. The comparison between experimental data [40] of the modulus and the simulation results of parallel-series model for triple-SMP with two transition behaviors

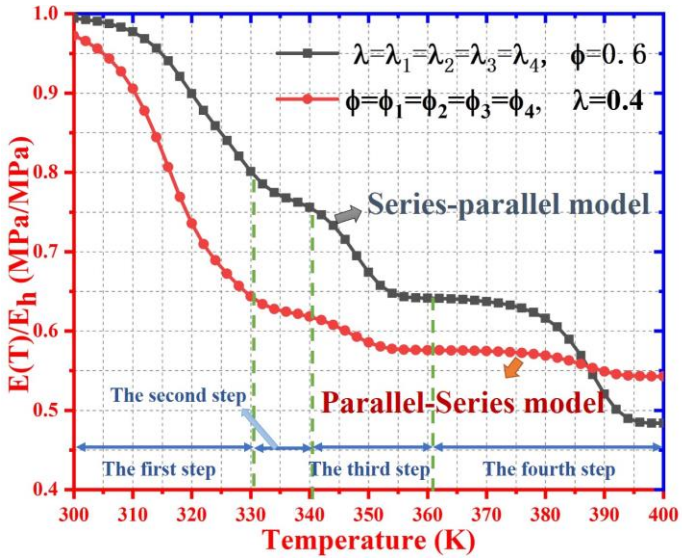

Figure 13. Numerical analysis results of the cooperative relaxation behavior happened in different temperature intervals based on the series-parallel model and the parallel-series model

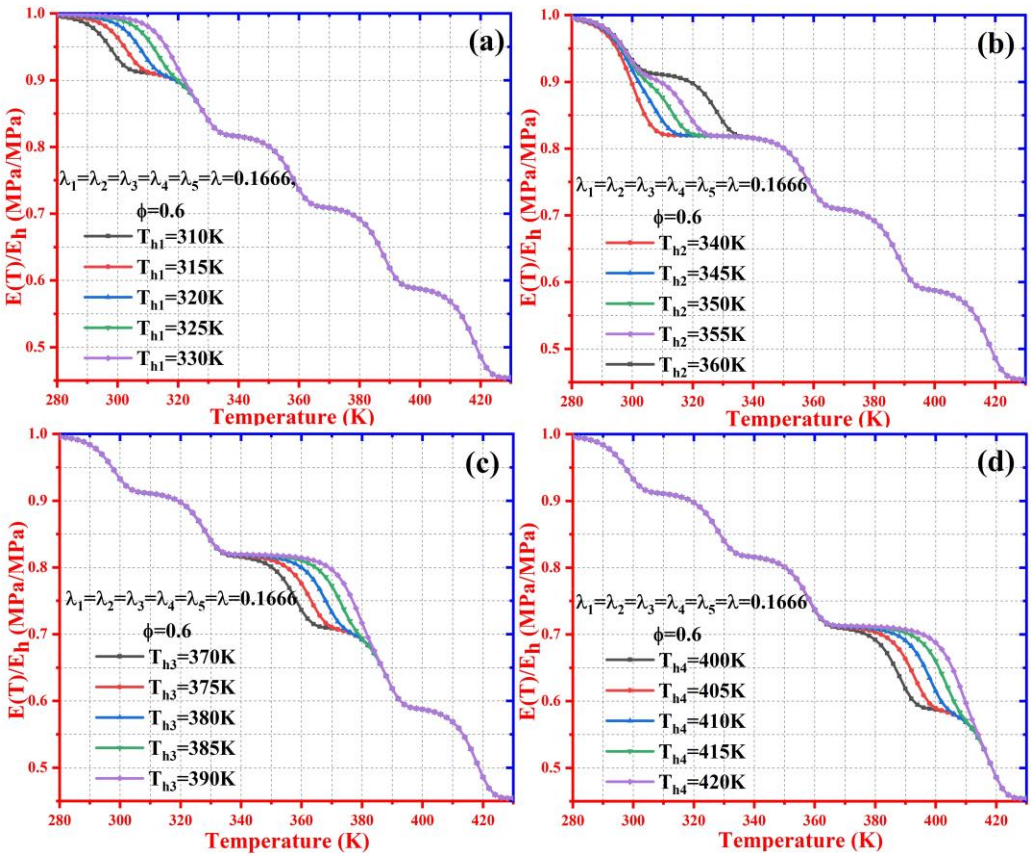

Figure 14. Numerical analysis results on the effect of the transition temperature interval between two soft segments on the multi-SME